Room Temperature Lasing from Semiconducting Single-Walled Carbon Nanotubes

Jia-Shiang Chen[1,2], Anushka Dasgupta[3], Darien J. Morrow[2], Ruggero Emmanuele[2], Tobin J. Marks[3,4], Mark C. Hersam[3,4,5], Xuedan Ma[1,2,6]*

[1]Northwestern-Argonne Institute of Science and Engineering, Northwestern University, Evanston, IL 60208, USA

[2]Center for Nanoscale Materials, Argonne National Laboratory, Lemont, Illinois 60439, United States

[3]Department of Materials Science and Engineering, and the Materials Research Center, Northwestern University, Evanston, Illinois 60208, United States

[4]Department of Chemistry, and the Materials Research Center, Northwestern University, Evanston, Illinois 60208, United States

[5]Department of Electrical and Computer Engineering, Northwestern University, Evanston, Illinois 60208, United States

[6]Consortium for Advanced Science and Engineering, University of Chicago, Chicago, Illinois 60637, United States

ABSTRACT

Miniaturized near-infrared semiconductor lasers that are able to generate coherent light with low energy consumption have widespread applications in fields such as optical interconnects,

neuromorphic computing and deep-tissue optogenetics. With optical transitions at near-infrared wavelengths, diameter-tunable electronic structures, and superlative optoelectronic properties, semiconducting single-walled carbon nanotubes (SWCNTs) are promising candidates for nanolaser applications. However, despite significant efforts in this direction and recent progress towards enhancing spontaneous emission from SWCNTs through Purcell effects, SWCNT-based excitonic lasers have not yet been demonstrated. Leveraging an optimized cavity-emitter integration scheme enabled by a self-assembly process, here we couple SWCNT emission to the whispering gallery modes supported by polymer microspheres, resulting in room temperature excitonic lasing with an average lasing threshold of 4.5 kW/cm^2. The high photostability of SWCNTs allows stable lasing for prolonged duration with minimal degradation. This experimental realization of excitonic lasing from SWCNTs, combined with their versatile electronic and optical properties that can be further controlled by chemical modification, offers far-reaching opportunities for tunable near-infrared nanolasers that are applicable for optical signal processing, in vivo biosensing, and optoelectronic devices.

KEYWORDS: single-walled carbon nanotubes, lasing, whispering gallery mode, microcavity, sp^3 quantum defects

INTRODUCTION

Semiconducting single-walled carbon nanotubes (SWCNTs) are one-dimensional cylindrical nanomaterials composed of covalently bonded carbon atoms forming hexagonal honeycomb

lattices. Depending on the relative orientations of the hexagonal lattices with respect to the nanotube axes, SWCNTs can possess distinct diameters and chiralities. Despite these structural diversity-induced variations in electronic structures,[1] optical properties of SWCNTs possess shared characteristics of strongly confined one-dimensional systems, where reduced dielectric screening and enhanced Coulomb interactions lead to the formation of stable excitons with large binding energies.[2, 3] These structural and electronic properties have enabled near-infrared optical emission from SWCNTs that spans the entire telecommunication band. Recent demonstrations of covalent chemical functionalization of SWCNTs provide further opportunities for modulating their optical transition energies.[4-7] Moreover, due to their exceptional electrical properties[8] as well as compatibility with photonic structures,[9, 10] SWCNTs are naturally suited for high-performance optoelectronic applications[11-13] including on-chip integration. For these reasons, significant research efforts have been devoted to the realization of SWCNT-based excitonic lasers that can operate at near-infrared wavelengths.[14-16]

Despite the early report of optical gain in SWCNTs,[14] the demonstration of their excitonic lasing has remained a longstanding elusive goal. While the optical gain threshold is primarily limited by the reabsorption losses of the gain material,[17] the realization of lasing requires a material that not only outcompetes reabsorption losses but also overcomes other detrimental nonradiative channels including ultrafast exciton-exciton annihilation processes.[18, 19] In an attempt to overcome these issues as well as the limited intrinsic gain coefficient of one-dimensional systems, SWCNTs have been integrated with photonic microcavities that can provide optical feedback. Although Purcell effect-induced photoluminescence (PL) enhancement has been demonstrated in these systems,[9, 10] the absence of SWCNT lasing signifies that material and cavity losses still outcompete stimulated emission.

In this study, we couple SWCNTs to polymer microspheres that support whispering gallery modes (WGMs) through a self-assembly approach. Our pump power-dependent PL spectroscopic studies and photon correlation measurements of the SWCNT/microsphere system reveal that the efficient spatial overlap between the gain material and the cavity modes enables the buildup of stimulated emission in the system and excitonic lasing from the SWCNTs. Moreover, the chemical functionalization-induced sp^3 dopants exhibit lower lasing thresholds compared to the pristine states. These findings suggest that by overlapping sufficient SWCNTs with optical cavity modes, stimulated emission can outcompete detrimental losses. In addition, careful chemical modification of the SWCNTs that is beneficial for improving their quantum efficiencies has the potential for pushing the lasing threshold to ultra-low limits.

RESULTS AND DISCUSSION

Here, we demonstrate room temperature lasing from SWCNTs by integrating them with polystyrene microspheres (Fig. 1a). Our design embraces two key factors to ensure that stimulated emission in SWCNTs surpasses material and cavity losses: 1) optimized coupling between the microcavity modes and SWCNTs, and 2) effective protection of the gain material from irradiation damage. Due to their dielectric contrast with the surrounding environment, polystyrene microspheres can support high-quality whispering gallery modes (WGMs), which are trapped, circulating modes of light due to total internal reflection at the boundaries of the dielectric structure. As can be seen in Fig. 1c and Fig. S1, WGMs are mainly confined at the edges of the microspheres. To enhance the spatial overlap between the WGMs and the gain material, we have adapted a swelling-deswelling encapsulation approach that has been used to decorate polymer beads with DNA molecules and nanoparticles.[20-22] This method enables the incorporation of

SWCNTs at the microsphere edges without introducing significant deleterious effects to the microcavities or the SWCNTs (Fig. 1b, also see Methods for details). Briefly, polar solvent-induced partial swelling of the polystyrene microspheres drives the SWCNTs, which are wrapped with hydrophobic polymers, to adhere onto and subsequently penetrate the surfaces of the microspheres due to van der Waals interactions between the SWCNTs and the microspheres. Following deswelling of the microspheres in ethanol, the SWCNTs become entrapped at the outer surfaces of the microspheres (Fig. S2e-2h).

In addition to the optimized spatial overlap between the WGMs and the SWCNTs, excellent alignment between the emission dipoles of the SWCNTs and electric fields of the microspheres can be expected. Specifically, WGMs in the microspheres consist of transverse electric (TE) modes that are oriented tangent to the microsphere surfaces (Fig. 1d inset), and transverse magnetic (TM) modes that are perpendicular to the surfaces. The band-edge emission dipoles of the SWCNTs are oriented along the tube axes.[23] Hence, despite the random distributions of the SWCNTs along the microsphere circumference, their emission dipoles will align well with the TE modes of the microspheres. This relative insensitivity of the coupling between the cavity modes and emission with respect to the SWCNT orientations allows the encapsulation of sufficient quantities of SWCNTs into the microcavities for achieving an adequate material gain volume. Moreover, embedding the SWCNTs in the polystyrene microspheres suppresses undesirable environmental perturbations to the SWCNTs,[24] thereby improving their photostability.

Aside from effective coupling between the SWCNTs and WGMs, quality (Q) factors and mode volumes of the WGMs are two other factors that have strong influence on the buildup of optical gain. The Q-factors of cavity modes determine the cavity photon lifetimes. Because the microcavity provides optical feedback, a large Q-factor implies that the cavity photons stay trapped

and interact with the gain material for a prolonged period of time, which is advantageous for achieving lasing. Cavity mode volumes are inversely proportional to Purcell factors,[25] hence the spontaneous lifetimes of the coupled PL.[26] While long cavity photon lifetimes and short spontaneous emission lifetimes are beneficial for the realization of lasing, they have opposite dependence on the microsphere diameter: a larger microsphere supports higher *Q*-factors and longer cavity photon lifetimes, but also possess larger mode volumes and less efficient Purcell effect. To balance the cavity *Q*-factors and mode volumes of the WGMs, we primarily use 5 μm diameter microspheres, although similar results can be obtained for 7 μm diameter microspheres (see Supporting Information I for cavity information). Fig. 1d shows the simulated resonance spectrum of the TE modes in a 5 μm diameter polystyrene microsphere. The quality *Q*-factor of the WGMs is approximately 3.5 - 4.0 x 10^3 in the spectral range of interest for this study. We utilize chirality-sorted pristine (6,5)-SWCNTs and those that are covalently functionalized with diazonium salts or iodoaniline as the gain material (see Methods for sample preparation details). Two characteristic PL peaks centered at near 1010 nm and 1170 nm can be observed upon chemical functionalization (Figs. 1e and 1f), each corresponding to the pristine E_{11} and functionalization-induced E_{11}^* states, respectively.[5, 27]

A pulsed laser with a pulse width of around 3.4 ps and a repetition frequency of 80 MHz is used to excite the SWCNTs at the phonon sideband of the E_{11} state at 820 nm. Upon integration of the SWCNTs into the microspheres, narrow PL peaks superimposed on the originally broad emission bands emerge (Fig. 2a). These sharp PL features result from coupling of the SWCNT spontaneous emission into the WGMs. The *Q*-factors of the microspheres after being integrated with SWCNTs are assessed from the linewidths of the narrow PL peaks at low pump powers: $Q = \lambda/\Delta\lambda$. The experimental *Q*-factors vary between 139 and 1629 with an average value of approximately 440

(Fig. S3). This reduction in the experimentally obtained *Q*-factor compared to the simulation results is likely caused by the decreased surface smoothness of the microspheres and occasional deformation in the spherical microspheres caused by the sample preparation process (Fig. S2). The coupling of the SWCNT emission into the microcavity modes is further manifested as cavity-mediated circulating emission around the microspheres (Fig. 2b). Specifically, when a diffraction limited laser beam irradiates a microsphere coated with SWCNTs (see Fig. S4 for the laser beam profile), instead of a localized emission spot resulting from direct laser excitation, delocalized emission can be observed from the entire microsphere. This is consistent with the simulated electric field distributions of the WGMs in Fig. 1c, and it strongly suggests that PL from the SWCNTs is coupled to the WGMs.

The intensities of the sharp PL peaks, which are extracted by fitting the PL spectra with multipeak Lorentzian functions to separate the narrow cavity emission from the broad background spontaneous emission of the SWCNTs (Fig. 2c), exhibit a sharp increase as the excitation power increases. Fig. 3a presents the integrated PL intensity of a representative narrow peak from Fig. 2a (~ 1028 nm) as a function of the pump power (i.e., the so-called light-in light-out or LL curve). The LL curve exhibits a soft threshold in the log-log scale, commonly observed for nanolasers with a large β factor, which is defined as the fraction of spontaneous emission coupled into the lasing cavity mode.[22, 28] When the excitation power exceeds a certain threshold, a noticeable change in the rising slope of the LL curve can be observed, with the PL intensity following a superlinear dependence on the pump power after this threshold value. This kind of rising slope change in the pump power-dependent PL intensity is observed in other cavity coupled peaks as well (see Fig. S7 for additional example), and is a key feature associated with the onset of stimulated emission in the cavity. In contrast, the intensity of the uncoupled background

spontaneous emission increases with the pump power with no apparent change in the rising slope until it saturates slightly at high powers (Fig. 3b).

The transition from spontaneous emission to lasing can be quantified by analyzing the LL curves using a coupled rate equation model (see Supporting Information V),[29] which takes into account radiative, nonradiative, and exciton-exciton annihilation processes of the SWCNTs as well as microcavity parameters.[19, 30] The β factor can be extracted by fitting LL curves with this coupled rate equation model. A large β factor indicates efficient coupling of spontaneous emission into the lasing cavity, which is beneficial for reducing the lasing threshold. We find that $\beta = 0.50$ is the best fit to the data shown in Fig. 3a, which is replotted in Fig. 3c together with the fitting curve as well as curves simulated using various β factors (see Fig. S5 for statistics of β factors of various nanolasers). This β value reflects that around 50% of the spontaneous emission from the SWCNTs is coupled into the WGM, likely benefiting from the large overlap between the WGMs and the integrated SWCNTs. It should be noted that saturation of the cavity emission at levels far above the threshold can be observed in some nanolasers (Fig. 3a and Fig. S7), which has been previously associated with extreme saturation of the excited states under pulsed excitations, thus resulting in smaller rising slopes.[28, 31] Our coupled rate equation model based on the pulsed excitation scheme used in this study accounts for this saturation behavior at high pump powers (see Supporting Information V for details).

Further evidence of lasing is provided from the analysis of the pump power-dependent cavity emission linewidth (Fig. 3a, orange dots). With increasing pump power, the spectral linewidth of the narrow cavity peak first drops sharply and then remains constant, indicating an increase in the temporal coherence, which is a hallmark of lasing phenomena.[28] This reduction in the PL linewidth with increasing pump power further attests to the onset of lasing beyond a certain threshold.

Additional confirmation of lasing from the SWCNT/microsphere system is achieved by performing second-order photon correlation ($g^{(2)}(\tau)$) measurements. Upon pulsed excitation, the area ratio, *R*, between the center peak at zero time-delay ($\tau = 0$) and the side peaks provides quantification of the emission photon statistics, with thermal radiation exhibiting super-Poissonian statistics ($R > 1$) and coherent lasing following Poissonian statistics ($R = 1$).[32, 33] For a $g^{(2)}(\tau)$ curve measured below the lasing threshold (bottom row, see Fig. S8 for the integrated areas of the peaks and Fig. S9 for another example), a bunching effect is observed with $R = 1.19 \pm 0.07$, signifying dominant spontaneous emission. In contrast, when the excitation power is raised to above the lasing threshold (Fig. 3d, upper row), the bunching peak disappears, and the photon emission statistics evolves from super-Poissonian to Poissonian with $R = 1.03 \pm 0.04$, evidencing the high temporal coherence that is characteristic of lasing.[32] We would like to note that the deviation of the *R* value from 2, which is expected for a typical thermal light source, has been observed in various types of nanolasers.[34-36] Due to the large *Q*-factors and small numbers of emitters in nanolasers, the transition from chaotic to coherent states broadens and occurs over a wide range of pump powers. Reduced photon fluctuations in such nanolasers can result in decreased *R* values.[35] In addition, the limited time resolution of the detectors used in this study may also contribute to the reduced *R* values.[35, 37]

These signatures, namely the concurrent observation of sublinear-to-superlinear transition in the PL intensity, linewidth narrowing, and super-Poissonian to Poissonian transition as a function of pump power, confirm lasing in the microsphere cavities. Similar lasing behavior was observed in ~ 40% of the measured microspheres. Moreover, these microsphere lasers possess high photostability with minimal degradation when subjected to prolonged continuous excitation at pump powers exceeding the lasing threshold (e.g., see Fig. S10a where 1 hour of illumination at

22.5 kW/cm^2, which is approximately three times the lasing threshold, leads to no significant degradation). The high photostability of the nanolasers is further confirmed by analyzing the pump power-dependent PL peak positions, which are expected to red shift in the presence of thermal degradation.[38] Minimal PL peak red-shift is observed even at high pump powers (Fig. S10b). We ascribe this high photostability to the superior thermal conductivity of SWCNTs[39] and the environmental protection provided by the polystyrene microspheres. Another significant feature of these SWCNT-based nanolasers is their wide coverage of the near-infrared wavelength range (Fig. 4a). Even wider tunability of the lasing wavelength is possible by utilizing SWCNTs of different chiralities and/or functionalized with diverse dopants as the gain material.[5, 7]

The lasing thresholds of the nanolasers are obtained from the LL curves, which vary between 0.24 and 13 kW/cm^2, with an average value of 4.5 kW/cm^2. This threshold value assumes that all of the pump light is injected into the nanolasers, although the exact lasing threshold corresponds to the pump light that is actually being absorbed by the gain material at the threshold. However, due to the difficulty in determining the exact input coupling efficiency of the pump light, we adopt the threshold values determined above, which provide upper bounds for the lasing threshold. This average threshold is smaller than the previously reported optical gain threshold of SWCNT thin films by nearly one order of magnitude,[14] likely caused by the single-chirality samples used in this study and the optical feedback provided by the microcavities. Indeed, the lasing threshold of the SWCNT nanolasers in this study is on par with early demonstrations of near-infrared lasers based on epitaxially grown III-V semiconductors coupled to plasmonic structures,[40] underscoring the potential of using SWCNTs as gain materials for near-infrared lasers.

If the lasing threshold is converted into the average number of excitons per SWCNT generated by the diffraction-limited laser beam,[41] an average value of $\langle N \rangle_{threshold} = 3.0$ is determined. This value

is larger than the gain threshold defined by the band-edge electronic state degeneracies of SWCNTs. From the analysis of quasi-Fermi potentials,[18] the lower limit of the gain threshold can be defined by $\langle N \rangle_{threshold} = g_e g_h/(g_e + g_h)$, where g_e and g_h are the band-edge degeneracy levels of the electron/hole states. For (6,5)-SWCNTs, both the electron and hole states of the lowest, optically active band are four-fold degenerate ($g_e = g_h = 4$),[2, 42] so the nominal minimum achievable $\langle N \rangle_{threshold}$ should be 2. Low-threshold lasing at pump powers below the gain threshold defined by the band-edge electronic state degeneracies has recently been demonstrated in semiconductor quantum dots by prohibiting nonradiative Auger recombination processes through composition and charge control.[18] In SWCNTs, the inevitable ultrafast exciton-exciton annihilation,[19, 30] together with other nonradiative recombination processes, constitutes significant loss channels that compete with stimulated emission, thus raising the lasing threshold to $\langle N \rangle_{threshold} = 3.0$. A careful inspection of the lasing threshold as a function of the lasing wavelength indicates that the E_{11} state on average ($\langle N \rangle_{threshold, E11} = 3.6$) has a greater lasing threshold than the E_{11}^* state ($\langle N \rangle_{threshold, E_{11}^*} = 2.1$, Fig. 4b). There are two factors that may contribute to this different lasing thresholds. Firstly, the functionalization-induced E_{11}^* states possess higher quantum efficiencies compared to the pristine E_{11} state.[5, 43] Thus, there are less contributions from nonradiative channels during the recombination process of the dopant states. Secondly, due to the three level energy states in the functionalized SWCNTs (ground, E_{11} and E_{11}^* states), excitons generated by optical excitation tend to get trapped at the doping sites due to fast exciton trapping rates. The long lifetimes of the E_{11}^* states can lead to accumulation of excitons at the E_{11}^* states and depletion of the ground state, thus assisting the formation of a population inversion and lowering the lasing threshold of the E_{11}^* state.[16, 44] Consequently, although the exciton-exciton annihilation might be more severe at the doping sites due to exciton localization, the improved quantum efficiency and ground state

depletion prevail and result in lower thresholds. These results suggest that the dopants in the chemically functionalized SWCNTs possess advantages for lasing, which should motivate further exploration of other chemical functionalization strategies in the future.

CONCLUSION

In summary, we have demonstrated lasing from SWCNTs coupled to WGMs in polystyrene microspheres. These SWCNT-based nanolasers exhibit stable lasing at near-infrared wavelengths over prolonged time with an average lasing threshold of 5.4 kW/cm^2 and 3.1 kW/cm^2 for the E_{11} and E_{11}^* state-based nanolasers, respectively. These results show that SWCNTs can serve as efficient gain material for near-infrared nanolasers when given sufficient optical feedback by photonic microcavities. We also find that the chemical functionalization-induced E_{11}^* state has a reduced threshold compared to the E_{11} state, suggesting the potential of further lowering the lasing threshold through careful SWCNT chemical modification. Future studies to improve the performance of SWCNT-based nanolasers would benefit from the development of more refined approaches for efficiently coupling SWCNT emission into high-quality cavities without compromising the optical and electronic properties of the SWCNTs. From the perspective of suppressing material losses, strategies such as surface passivation or environmental treatment to remove nonradiative channels and reduce inhomogeneous broadening,[24, 45] as well as utilizing charged states to bleach the ground state,[18, 46] may also lower the lasing thresholds of SWCNT-based nanolasers. Finally, the development of electrically injected SWCNT nanolasers would facilitate their practical implementation in integrated optoelectronic devices.[40] Overall, the demonstration of room temperature SWCNT lasing in this work is likely to reinvigorate efforts to incorporate SWCNTs into a broad range of photonic technologies.

METHODS

Chirality sorting and chemical functionalization of SWCNTs. (6,5)-enriched SWCNT samples (1 mg/mL) were obtained by first dispersing the raw powders (CoMoCAT SG65i, Sigma-Aldrich) in 1 wt% aqueous sodium dodecyl sulfate (SDS) solution by tip sonication for 1 h while cooling in an ice bath. Impurities were removed by subsequent ultracentrifugation at 125,000g for 1.5 hours. The resultant supernatant was extracted for chirality sorting and chemical functionalization. In particular, we used two different dopants (4-nitrobenzene diazonium salts and 4-iodoaniline) for creating sp^3 quantum defects in SWCNTs.[5, 47] For chemical functionalization of the SWCNTs with diazonium salts, a stock solution of 5 mM 4-nitrobenzene diazonium tetrafluoroborate (NBDT, Sigma-Aldrich) was added to the SWCNT suspension to achieve an approximate [C]:[NBDT] ratio of 300:1. This reaction occurred at room temperature in the dark with stirring, and the reaction progress was monitored by measuring the PL spectra of the solution until a desirable E_{11}^*/E_{11} ratio was reached. For chemical functionalization with photoexcited aromatic reactants, stock solutions of 0.2 M 4-iodoaniline (Sigma-Aldrich) in acetonitrile and 0.3 M sodium hydroxide were added to the diluted SWCNT suspension to achieve final concentrations of ~ 2 mM and ~ 0.1 mM, respectively. The solutions were then sparged with Ar gas for 1 h to remove dissolved O_2. This reaction proceeded under UV irradiation (~ 300 nm, 0.6 mW/mm^2) for 2 h at room temperature with stirring. Once the desired doping level was achieved in both functionalization schemes, the doped-SWCNT solutions were immediately filtered by vacuum filtration on a borosilicate filter and washed with deionized water and isopropanol in an effort to remove excess surfactants and unreacted dopants. The filter with doped-SWNCTs was then dried overnight in a vacuum oven at 100 °C. Finally, the doped SWCNTs were removed from the filter

and selectively sorted for the (6,5) chirality by dispersing them in 1 mg/mL poly[(9,9-dioctylfluorenyl-2,7-diyl)-alt-co-(6,6')-(2,2'-bipyridine)] (PFO-BPy, American Dye Source, ADS153UV) in toluene via tip sonication for 1 h followed by centrifugation at 15,000 rpm for 10 min.

Fabrication of SWCNT-polystyrene nanolasers. The integration of SWCNTs with polystyrene microspheres was achieved in solution by adding 15 μL of highly concentrated SWCNT/toluene suspension (optical density above 1 at the E_{11} absorption peak) and 3 μL of polystyrene microspheres in deionized water (10 wt%) into 126 μL butanol. The mixture was then sonicated and vortexed for 5 s. Homogeneous coating of SWCNTs on the polystyrene microsphere surfaces was controlled by changing the stirring condition from 120 rpm for 1.5 h to 60 rpm for 1.5 h. The resulting mixture was then incubated without stirring for 1 h at room temperature. Finally, the SWCNT-polystyrene nanolasers were purified by centrifugation at 3,000 rpm for 4 min followed by washing with ethanol. This purification process was repeated three times.

Numerical simulations. Resonance spectra, quality factors, and electric field profiles of the polystyrene microspheres were calculated using the Finite-Difference Time-Domain method (FDTD, Lumerical). The simulation mesh size was set to be 10 nm or 20 nm, depending on the sizes of the microspheres. Two stacked electric dipoles oriented perpendicular to each other were used as the sources to excite the TE and TM modes in the microspheres.

Optical measurements. Suspensions of polystyrene microspheres integrated with SWCNTs were diluted and spin-coated onto pre-cleaned cover slides and loaded onto a home-built confocal laser scanning microscope for optical measurements. The SWCNTs were excited at the phonon sideband of the E_{11} state at 820 nm using a pulsed laser (~ 3.4 ps, 80 MHz) at various pump powers. A microscope objective (40x, NA=0.95) was used to focus the pump beam onto the samples and

collect the emission. Photoluminescence images and spectra were recorded using a two-dimensional InGaAs array installed on a 327 mm spectrograph. Gratings with dispersions of 150 and 300 grooves/mm were used. The slide width was set to be around 20 μm, which yields spectral resolutions of around 0.27 - 0.55 nm. Scanning photoluminescence images and time traces were measured by directing the photoluminescence signal to single photon counting detectors. For second-order photon correlation measurements, the selected WGM mode photoluminescence emission was spectrally filtered by a combination of longpass and shortpass filters, and then split by a 50:50 beam splitter and focused onto two identical single photon counting detectors in a Hanbury-Brown and Twiss geometry. Single photon events were recorded using time-correlated photon counting electronics (PicoQuant).

ASSOCIATED CONTENT

Supporting Information.

The following files are available free of charge:

Optical micrographs and transmission electron microscopes images; finite-difference time-domain (FDTD) simulations; distributions of the experimentally determined quality factors; spatial profile of the excitation laser beam; description of the coupled rate equation model; additional example of SWCNT-based nanolaser; second-order photon correlation spectroscopy; photostability of SWCNT-based nanolasers.

AUTHOR INFORMATION

Corresponding Author

*Email: xuedan.ma@anl.gov

Notes

The authors declare no competing final interest.

ACKNOWLEDGMENT

This research was primarily supported by the Center for Molecular Quantum Transduction, an Energy Frontier Research Center funded by the U.S. Department of Energy, Office of Science, Office of Basic Energy Sciences, under award no. DE-SC0021314 (sample preparation and optical measurements) and by the U.S. Department of Energy, Office of Science, Office of Basic Energy Sciences, Materials Science and Engineering Division (cavity simulation). A.D. acknowledges a National Science Foundation Graduate Research Fellowship. X.M. acknowledges support from the National Science Foundation DMR Program under award no. DMR-1905990. This work was performed, in part, at the Center for Nanoscale Materials, a U.S. Department of Energy Office of Science User Facility, and supported by the U.S. Department of Energy, Office of Science, under Contract No. DE-AC02-06CH11357. In addition, this work was performed, in part, at the National Science Foundation Materials Research Science and Engineering Center at Northwestern University under award no. DMR-1720319.

REFERENCES

1. Bachilo, S. M.; Strano, M. S.; Kittrell, C.; Hauge, R. H.; Smalley, R. E. & Weisman, R. B. Structure-Assigned Optical Spectra of Single-Walled Carbon Nanotubes. *Science* **2002,** *298*, 2361-2366.

2. Spataru, C. D.; Ismail-Beigi, S.; Capaz, R. B. & Louie, S. G. Theory and Ab Initio Calculation of Radiative Lifetime of Excitons in Semiconducting Carbon Nanotubes. *Phys. Rev. Lett.* **2005,** *95*, 247402.

3. Wang, F.; Dukovic, G.; Brus, L. E. & Heinz, T. F. The optical resonances in carbon nanotubes arise from excitons. *Science* **2005,** *308*, 838-841.

4. Ghosh, S.; Bachilo, S. M.; Simonette, R. A.; Beckingham, K. M. & Weisman, R. B. Oxygen doping modifies near-infrared band gaps in fluorescent single-walled carbon nanotubes. *Science* **2010,** *330*, 1656-1659.

5. Piao, Y.; Meany, B.; Powell, L. R.; Valley, N.; Kwon, H.; Schatz, G. C. & Wang, Y. Brightening of carbon nanotube photoluminescence through the incorporation of sp^3 defects. *Nat. Chem.* **2013,** *5*, 840-845.

6. Chiu, C. F.; Saidi, W. A.; Kagan, V. E. & Star, A. Defect-induced near-infrared photoluminescence of single-walled carbon nanotubes treated with polyunsaturated fatty acids. *J. Am. Chem. Soc.* **2017,** *139*, 4859-4865.

7. He, X. et al. Tunable room-temperature single-photon emission at telecom wavelengths from sp3 defects in carbon nanotubes. *Nat. Photonics* **2017,** *11*, 577-582.

8. Avouris, P.; Chen, Z. & Perebeinos, V. Carbon-based electronics. *Nat. Nanotechnol.* **2007,** *2*, 605-615.

9. Ma, X. & Htoon, H. Tailoring the photophysical properties of carbon nanotubes by photonic nanostructures. *Mod. Phys. Lett. B* **2015,** *29*, 1530004.

10. He, X.; Htoon, H.; Doorn, S. K.; Pernice, W. H. P.; Pyatkov, F.; Krupke, R.; Jeantet, A.; Chassagneux, Y. & Voisin, C. Carbon nanotubes as emerging quantum-light sources. *Nat. Mater.* **2018,** *17*, 663-670.

11. He. X., Gao, W., Xie, L., Li, B., Zhang, Q., Lei, S., Robinson, J. M., Hároz, E. H., Doorn, S. K., Wang, W/, Vajtai, R., Ajayan, P. M., Wade Adams, W., Hauge, R. H. & Kono, J. Wafer-scale monodomain films of spontaneously aligned single-walled carbon nanotubes. *Nat. Nanotechnol.* **2016,** *11*, 633-638.

12. Graf, A.; Held, M.; Zakharko, Y.; Tropf, L.; Gather, M. C. & Zaumseil, J. Electrical pumping and tuning of exciton-polaritons in carbon nanotube microcavities. *Nat. Mater.* **2017,** *16*, 911-917.
13. Khasminskaya, S. et al. Fully integrated quantum photonic circuit with an electrically driven light source. *Nat. Photonics* **2016,** *10*, 727-732.
14. Gaufrès, E.; Izard, N.; Le Roux, X.; Marris-Morini, D.; Kazaoui, S.; Cassan, E. & Vivien, L. Optical gain in carbon nanotubes. *Appl. Phys. Lett.* **2010,** *96*, 231105.
15. Miura, R.; Imamura, S.; Ohta, R.; Ishii, A.; Liu, X.; Shimada, T.; Iwamoto, S.; Arakawa, Y. & Kato, Y. K. Ultralow mode-volume photonic crystal nanobeam cavities for high-efficiency coupling to individual carbon nanotube emitters. *Nat. Commun.* **2014,** *5*, 5580.
16. Sykes, J. E.; Kim, M.; Wu, X.; Wiederrecht, G. P.; Peng, L.; Wang, Y.; Gosztola, D. J. & Ma, X. Ultrafast exciton trapping at sp*3* quantum defects in carbon nanotubes. *ACS Nano* **2019,** *13*, 13264-13270.
17. Park, Y.-S.; Roh, J.; Diroll, B. T.; Schaller, R. D. & Klimov, V. I. Colloidal quantum dot lasers. *Nat. Rev. Mater.* **2021,** *6*, 382-401.
18. Kozlov, O. V.; Park, Y.-S.; Roh, J.; Fedin, I.; Nakotte, Y. & Klimov, V. I. Sub–single-exciton lasing using charged quantum dots coupled to a distributed feedback cavity. *Science* **2019,** *365*, 672-675.
19. Ma, X.; Roslyak, O.; Duque, J. G.; Pang, X.; Doorn, S. K.; Piryatinski, A.; Dunlap, D. H. & Htoon, H. Influences of exciton diffusion and exciton-exciton annihilation on photon emission statistics of carbon nanotubes. *Phys. Rev. Lett.* **2015,** *115*, 017401.
20. Kim, A. J.; Manoharan, V. N. & Crocker, J. C. Swelling-based method for preparing stable, functionalized polymer colloids. *J. Am. Chem. Soc.* **2005,** *127*, 1592-1593.
21. Oh, J. S.; Wang, Y.; Pine, D. J. & Yi, G.-R. High-density PEO-b-DNA brushes on polymer particles for colloidal superstructures. *Chem. Mater.* **2015,** *27*, 8337-8344.
22. Fernandez-Bravo, A. et al. Continuous-wave upconverting nanoparticle microlasers. *Nat. Nanotechnol.* **2018,** *13*, 572-577.
23. Kilina, S.; Tretiak, S.; Doorn, S. K.; Luo, Z.; Papadimitrakopoulos, F.; Piryatinski, A.; Saxena, A. & Bishop, A. R. Cross-polarized excitons in carbon nanotubes. *Proc. Natl. Acad. Sci.* **2008,** *13*, 6797-6802.
24. Walden-Newman, W.; Sarpkaya, I. & Strauf, S. Quantum light signatures and nanosecond spectral diffusion from cavity-embedded carbon nanotubes. *Nano Lett.* **2012,** *12*, 1934-1941.

25. Purcell, E. M. Spontaneous emission probabilities at radio frequencies. *Phys. Rev. Lett.* **1946,** *69*, 681.

26. Peng, L.; Wang, X.; Coropceanu, I.; Martinson, A. B.; Wang, H.; Talapin, D. V.; Ma, X. Titanium Nitride Modified Photoluminescence from Single Semiconductor Nanoplatelets. *Adv. Funct. Mater.* **2020,** *30*, 1904179.

27. Ma, X.; Adamska, L.; Yamaguchi, H.; Yalcin, S. E.; Tretiak, S.; Doorn, S. K. & Htoon, H. Electronic structure and chemical nature of oxygen dopant states in carbon nanotubes. *ACS Nano* **2014,** *8*, 10782-10789.

28. Paik, E. Y.; Zhang, L.; Burg, G. W.; Gogna, R.; Tutuc, E. & Deng, H. Interlayer exciton laser of extended spatial coherence in atomically thin heterostructures. *Nature* **2019,** *576*, 80-84.

29. Bjork. G. & Yamamoto, Y. Analysis of semiconductor microcavity lasers using rate equations. *IEEE J. Quant. Electon.* **1991,** *27*, 2386-2396.

30. Ma, Y.-Z.; Valkunas, L.; Dexheimer, S. L.; Bachilo, S. M. & Fleming, G. R. Femtosecond Spectroscopy of Optical Excitations in Single-Walled Carbon Nanotubes: Evidence for Exciton-Exciton Annihilation. *Phys. Rev. Lett.* **2005,** *94*, 157402.

31. Fernandez-Bravo, A. et al. Ultralow-threshold, continuous-wave upconverting lasing from subwavelength plasmons. *Nat. Mater.* **2019,** *18*, 1172-1176.

32. Lu, Y.-J. et al. Plasmonic nanolaser using epitaxially grown silver film. *Science* **2012,** *337*, 450-453.

33. Chow, W. W.; Jahnke, F. & Gies, C. Emission properties of nanolasers during the transition to lasing. *Light Sci. Appl.* **2014,** *3*, e201.

34. W. E. Hayenga, H. Garcia-Gracia, H. Hodaei, C. Reimer, R. Morandotti, P. LiKamWa, M. Khajavikhan. Second-order coherence properties of metallic nanolasers. *Optica* **2016,** *3*, 1187-1193.

35. S. M. Ulrich, C. Gies, S. Ates, J. Wiersig, S. Reitzenstein, C. Hofmann, A. Löffler, A. Forchel, F. Jahnke, P. Michler. Photon Statistics of Semiconductor Microcavity Lasers. *Phys. Rev. Lett.* **2007,** *98*, 043906.

36. S. H. Pan, Q. Gu, A. El Amili, F. Vallini, Y. Fainman. Dynamic hysteresis in a coherent high-β nanolaser. *Optica* **2016,** *3*, 1260-1265.

37. Loudon, R. *The quantum theory of light*, Third Edition; Oxford University Press: New York, 2003; Page 233-286.

38. Yoshino, K.; Kato, T.; Saito, Y.; Shitaba, J.; Hanashima, T.; Nagano, K.; Chiashi, S. & Homma, Y. Temperature Distribution and Thermal Conductivity Measurements of Chirality-Assigned Single-Walled Carbon Nanotubes by Photoluminescence Imaging Spectroscopy. *ACS Omega* **2018,** *3*, 4352-4356.

39. Balandin, A. A. Thermal properties of graphene and nanostructured carbon materials. *Nat. Mater.* **2011,** *10*, 569-581.

40. Ma, R.-M. & Oulton, R. F. Applications of nanolasers. *Nat. Nanotechnol.* **2019,** *14*, 12-22.

41. Ma, X.; Diroll, B. T.; Cho, W.; Fedin, I.; Schaller, R. D.; Talapin, D. V.; Gray, S. K.; Wiederrecht, G. P. & Gosztola, D. J. Size-Dependent Biexciton Quantum Yields and Carrier Dynamics of Quasi-Two-Dimensional Core/Shell Nanoplatelets. *ACS Nano* **2017,** *11*, 9119-9127.

42. C. Voisin, S. Berger, S. Berciaud, H. Yan, J.-S. Lauret, G. Cassabois, P. Roussignol, J. Hone, T. F. Heinz. Excitonic signatures in the optical response of single-wall carbon nanotubes. *Phys. Status Solidi B* **2012,** *249*, 900-906.

43. Miyauchi, Y.; Iwamura, M.; Mouri, S.; Kawazoe, T.; Ohtsu, O. & Matsuda, M. Brightening of excitons in carbon nanotubes on dimensionality modification. *Nat. Photonics* **2013,** *7*, 715-719.

44. Iwamura, M.; Akizuki, N.; Miyauchi, Y.; Mouri, S.; Shaver, J.; Gao, Z.; Cognet, L.; Lounis, B.; Matsuda, K. Nonlinear Photoluminescence Spectroscopy of Carbon Nanotubes with Localized Exciton States. *ACS Nano* **2014,** *8*, 11254-11260.

45. Saha, A.; Gifford, B. J.; He, X.; Ao, G.; Zheng, M.; Kataura, H.; Htoon, H.; Kilina, S.; Tretiak, S. & Doorn, S. K. Narrow-band single-photon emission through selective aryl functionalization of zigzag carbon nanotubes. *Nat. Chem.* **2018,** *10*, 1089-1095.

46. Santos, S. M.; Yuma, B.; Berciaud, S.; Shaver, J.; Gallart, M.; Gilliot, P.; Cognet, L. & Lounis, B. All-Optical Trion Generation in Single-Walled Carbon Nanotubes. *Phys. Rev. Lett.* **2011,** *107*, 187401.

47. Zheng, Y.; Bachilo, S. M.; Weisman, R. B. Photoexcited Aromatic Reactants Give Multicolor Carbon Nanotube Fluorescence from Quantum Defects. *ACS Nano* **2020,** *14*, 715-723.

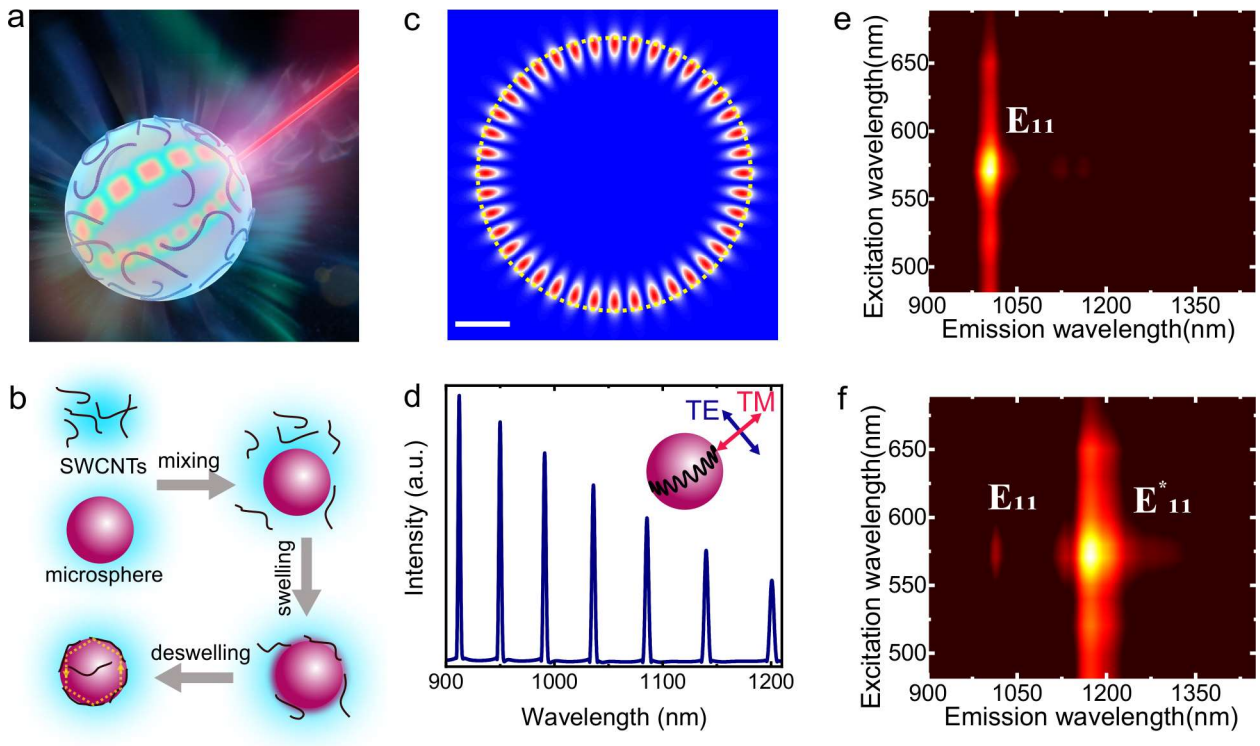

Figure 1. (a, b) Schematic (a) and preparation method (b) of the SWCNT nanolasers. (c, d) Simulated electric field $|\mathbf{E}|^2$ distribution (c) and resonance spectrum (d) of the transverse electric mode in a 5 μm diameter polystyrene microsphere. The scale bar in (c) is 1 μm. The inset in (d) indicates the orientations of the electric field **E** in the transverse electric (TE) and magnetic (TM) modes with respect to the microsphere. (e, f) Photoluminescence excitation spectroscopy of the pristine (e) and functionalized (f) (6,5)-SWCNTs.

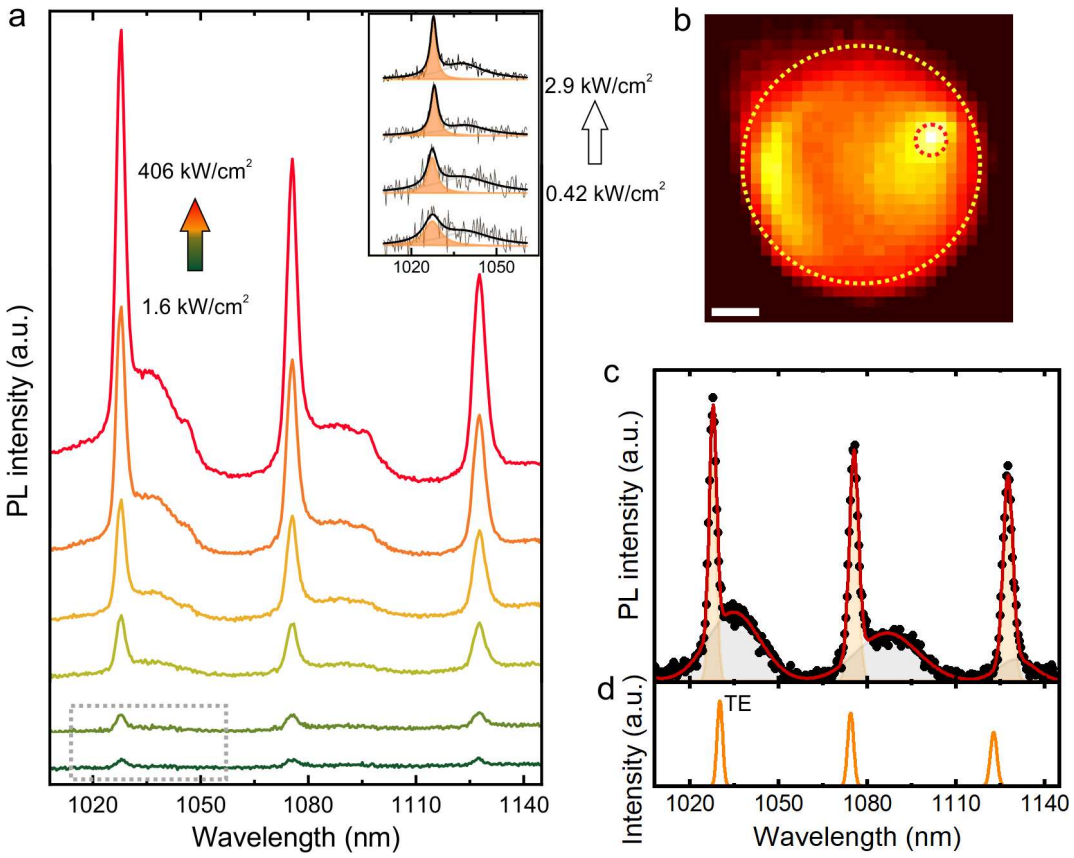

Figure 2. (a) Pump power-dependent photoluminescence spectra of chemically functionalized SWCNTs coupled to a polystyrene microsphere. The inset corresponds to the region marked by the dashed line. The black curves in the inset are two-peak Lorentzian fits to the spectra. (b) Wide-field photoluminescence image of a dopant-based SWCNT nanolaser. In the wide-field image mode, the diffraction-limited laser beam illuminates the nanolaser at the indicated location (red circle), and the photoluminescence from the entire nanolaser is recorded simultaneously. The yellow circle indicates the location of the polystyrene microsphere. The scale bar is 1 μm. (c) A representative photoluminescence spectrum (dots) from the nanolaser in (a) with a multipeak fit (solid line). (d) Simulated TE resonance modes supported by a 5.4 μm diameter polystyrene microsphere.

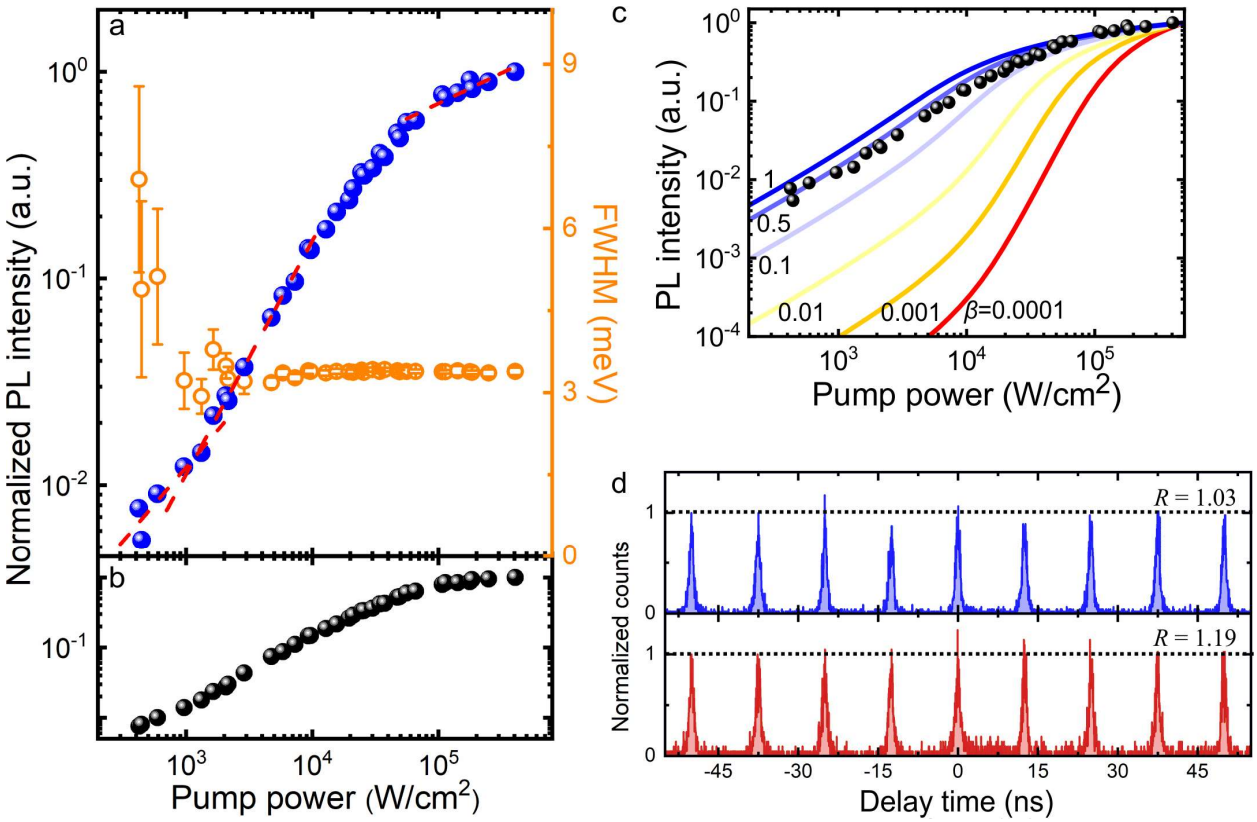

Figure 3. (a) Normalized pump power-dependent photoluminescence intensity (blue dots) and linewidth (orange circles) extracted from photoluminescence spectra of chemically functionalized SWCNTs coupled to a polystyrene microsphere. The corresponding peak wavelength is 1028 nm. A change in the pump-dependent slopes of the intensity and linewidth can be observed at similar pump powers, indicating the transition from spontaneous emission to stimulated emission. The red lines are power law fits to the intensity data in the different pump power regions. (b) Normalized pump power-dependent photoluminescence intensity of the uncoupled background spontaneous emission. (c) Normalized pump power-dependent photoluminescence intensity (i.e., the LL curve, dots) and a fit using the coupled rate equations with β = 0.50. Simulated curves with β = 1, 0.1, 0.01, 0.001, and 0.0001 are also shown. (d) Second-order photon correlation spectroscopy ($g^{(2)}(\tau)$) of a pristine SWCNT-based nanolaser at pump powers below (bottom) and above (top) the lasing

threshold. *R* values of 1.03 ± 004 and 1.19 ± 007 are extracted from the top and bottom curves, respectively.

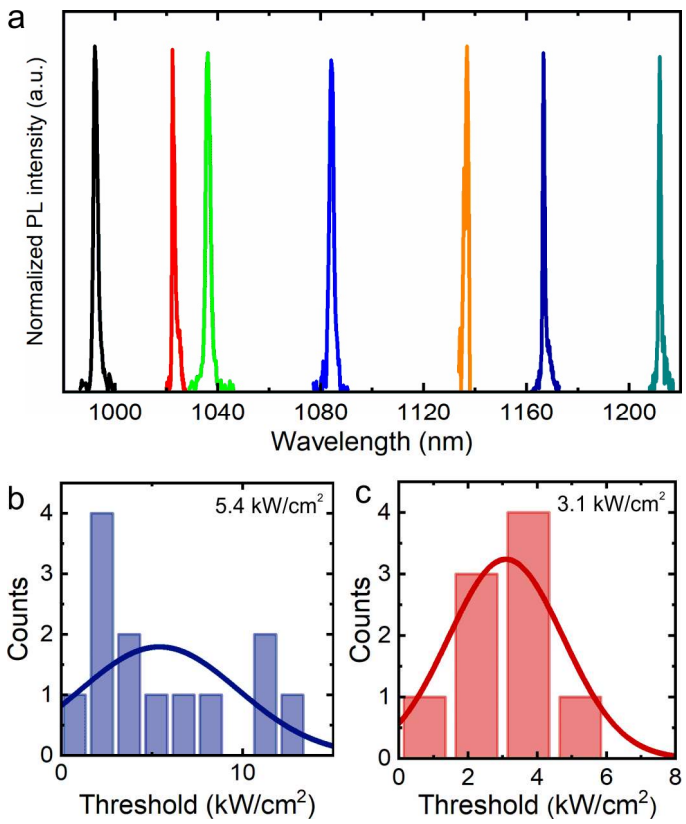

Figure 4. (a) Emission spectra of representative SWCNT-based nanolasers spanning a wide wavelength range. (b, c) Histograms of the lasing thresholds of the E_{11} (b) and E_{11}^{*} state-based (c) nanolasers. The average lasing thresholds are estimated to be 5.4 kW/cm^2 ($\langle N \rangle_{threshold}$ = 3.6) and 3.1 kW/cm^2 ($\langle N \rangle_{threshold}$ = 2.1) for the E_{11} and E_{11}^{*} state-based nanolasers, respectively.

TOC

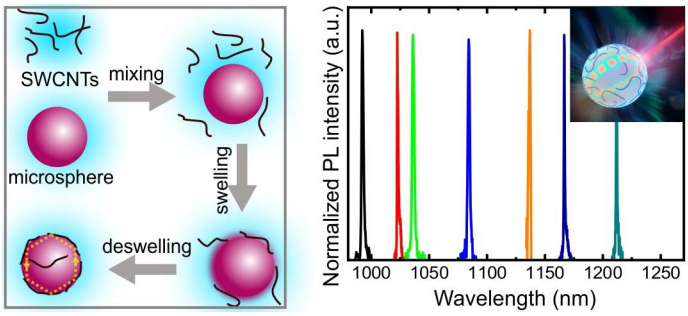
SWCNTs
mixing
microsphere
swelling
deswelling
Normalized PL intensity (a.u.)
1000
1050
1100
1150
1200
1250
Wavelength (nm)